

THE BE/X-RAY BINARY SWIFT J1626.6–5156 AS A CYCLOTRON LINE SOURCE

M. E. DECESAR

Department of Astronomy and
University of Maryland, College Park, MD 20742, USA

AND

P. T. BOYD

Center for Research and Exploration in Space Science and Technology and NASA Goddard Space Flight Center
Code 661, Greenbelt, MD 20771, USA
Currently NASA Headquarters and
300 E Street SW, Mail Suite 3W39, Washington, DC 20546, USA

AND

K. POTTSCHMIDT

Center for Research and Exploration in Space Science and Technology and NASA Goddard Space Flight Center and
Code 661, Greenbelt, MD 20771, USA

AND

J. WILMS

Dr. Karl Remeis-Sternwarte
Astronomisches Institut der Universität Erlangen-Nürnberg, Sternwartstr. 7, 96049 Bamberg, Germany
Erlangen Centre for Astroparticle Physics and
Universität Erlangen-Nürnberg, Erwin-Rommel-Str. 1, 91058 Erlangen, Germany

AND

S. SUCHY

Center for Astrophysics and Space Sciences and
University of California, San Diego, 9500 Gilman Dr., La Jolla, CA 92093-0424, USA

AND

M. C. MILLER

Department of Astronomy
University of Maryland, College Park, MD 20742, USA
Maryland Astronomy Center for Theory and Computation and
University of Maryland, College Park, MD 20742, USA

Draft version August 3, 2009

ABSTRACT

Swift J1626.6–5156 is a Be/X-ray binary that was in outburst from December 2005 until November 2008. We have examined RXTE/PCA and HEXTE spectra of three long observations of this source taken early in its outburst, when the PCA 2 – 20 keV count rate was $> 70 \text{ counts s}^{-1} \text{ PCU}^{-1}$, as well as several combined observations from different stages of the source’s life. The spectra are best fit with an absorbed cut-off power law with a $\sim 6.4 \text{ keV}$ iron emission line and a Gaussian optical depth absorption line at $\sim 10 \text{ keV}$. We present strong evidence that this absorption feature is actually a cyclotron resonance scattering feature, making Swift J1626.6–5156 a new candidate cyclotron line source. The redshifted energy of $\sim 10 \text{ keV}$ implies a magnetic field strength of $\sim 8.6(1+z) \times 10^{11} \text{ G}$ in the region of the accretion column close to the magnetic poles where the cyclotron line is produced. Phase-resolved spectroscopy reveals the second harmonic of the fundamental cyclotron line. There is a significant positive correlation between the fundamental cyclotron energy and the source luminosity.

Subject headings:

1. INTRODUCTION

The high-mass X-ray binary (HMXB) Swift J1626.6–5156 was discovered in outburst by the Swift Burst Alert Telescope (BAT) on 18 December 2005 (Krimm et al. 2005). It was soon recognized to be an X-ray pulsar with a $\sim 15 \text{ s}$ spin period (Palmer et al. 2005), and its companion was classified as a Be

star (Negueruela & Marco 2006). Shortly after the discovery, the Rossi X-ray Timing Explorer (RXTE) began monitoring the source, and has continued to do so for nearly four years. The categorization of Swift J1626.6–5156 as a Be/X-ray binary (BeX) places it in a group that comprises most of the HMXB population, so we will describe it in terms associated with that group of objects. Its 2 – 20 keV PCA light curve is shown in Figure 1, spanning the beginning of RXTE’s monitoring in January 2006 to the present.

Swift J1626.6–5156 was discovered during a Type II outburst, which is thought to occur when the Be star’s circumstellar disk expands and temporarily engulfs the

Electronic address: decesar@astro.umd.edu
Electronic address: patricia.t.boyd@nasa.gov
Electronic address: katja@milkyway.gsfc.nasa.gov
Electronic address: joern.wilms@sternwarte.uni-erlangen.de
Electronic address: ssuchy@ucsd.edu
Electronic address: miller@astro.umd.edu

neutron star, leading to enhanced accretion and therefore a large increase in X-ray emission (Coe 2000 and references therein). Reig et al. (2008) describe the exponential decay of the outburst and the flaring behavior that occurred in the weeks immediately following the discovery. Following JD 2453800 (2006 March 5), there is additional flaring that has not yet been studied, to our knowledge. After this, the source transitions into an epoch of long-term, quasi-periodic X-ray oscillations (Reig et al. 2008). A Lomb-Scargle periodogram (Lomb 1976, Scargle 1982) of the light curve reveals an oscillation period from \sim JD 2454000 – 2454350 (2006 September – 2007 September) of \sim 47 days, and from \sim JD 2454350 – 2454790 (2007 September – 2008 November) of \sim 3/2 this, or \sim 72.5 days (DeCesar et al. 2009). This behavior may be explained by Type I outbursts, caused when the neutron star, on an eccentric orbit, passes through the circumstellar disk at periastron; however, if this is the cause, we suggest that the orbital period may be half the observed initial period, or \sim 23 days. Whether or not the quasi-periodic flux increases are caused by Type I outbursts must be confirmed by establishment of the source’s orbital parameters. If the orbit is not causing the flux oscillations, it may be that the neutron star hosts a precessing, warped accretion disk, as in the case of Her X-1 (Gerend & Boynton 1976) or SMC X-1 (Trowbridge et al. 2007), though an explanation of the factor of 3/2 difference between the two periodicities observed is not obvious. Other phenomena that may lead to non-orbital periodicities in X-ray binaries are reviewed by Priedhorsky & Holt (1987).

On JD 2454791 (2008 November 11), the oscillatory behavior ceased, and the X-ray 2 – 20 keV count rate from Swift J1626.6–5156 dropped to \sim 1 count s^{-1} . The long-term behavior of the source is beyond the scope of this letter, but will be discussed in a following paper.

Many BeX and other HMXB systems harbor neutron stars with very strong magnetic fields, typical strengths being $\sim 10^{11-13}$ G, and some of these systems exhibit cyclotron resonance scattering features (CRSFs, or cyclotron lines). At the time of writing, there are 13 neutron star X-ray binaries with confirmed CRSFs (Heindl et al. 2004, Coburn et al. 2006, Lutovinov & Tsygankov 2008, and references therein), 7 of which are transients (Swift J1626.6–5156 being the 8th); of the transients, 3 systems are BeX (Swift J1626.6–5156 being the 4th), one (MXB 0656–072) is an Oe/X-ray binary (OeX), one (Her X-1) is a low-mass X-ray binary (LMXB), and the rest are HMXBs with a B star accompanying the NS. The fundamental cyclotron line energy $E_{\text{cyc}} \approx 11.6 B_{12} (1+z)^{-1}$ keV, where $B_{12} = B/(10^{12}$ G) and z is the surface gravitational redshift. Assuming a reasonable value of z corresponding to a typical neutron star mass of $1.4M_{\odot}$ allows a direct calculation of B in the region local to the magnetic pole, where the cyclotron lines are produced. Observing cyclotron lines in the spectra of these systems is the only direct way to measure the magnetic field strengths of neutron stars.

In this letter, we discuss the discovery of a CRSF in the spectrum of Swift J1626.6–5156. A subsequent paper will take a detailed look at the long-term spectral and temporal variability. In §2, we describe our data reduction and analysis techniques. §3 presents results

from modeling the broad band X-ray spectra, including CRSFs and other spectral properties of the source. We summarize our findings and compare Swift J1626.6–5156 with other cyclotron line sources in §4, and conclude in §5.

2. OBSERVATIONS AND DATA ANALYSIS

For this analysis, we used data from the Proportional Counter Array (PCA; Jahoda et al. 2006) and High Energy X-ray Timing Experiment (HEXTE; Rothschild et al. 1998) onboard RXTE that were taken between December 2005 and April 2009. From HEXTE, we used spectra from the B cluster only; the A cluster has stopped rocking¹, which makes background calculations difficult. We extracted spectra in standard2 mode from the top layer of each PCA Proportional Counter Unit (PCU) separately. We then combined all spectra from a given observation into one, following the recipe in the RXTE Cookbook² and excluding data taken within 10 min of the South Atlantic Anomaly. For additional settings like elevation and electron ratio, and for a more detailed description of the data reduction procedure, see Wilms et al. (2006). We considered the PCA energy range 4 – 22 keV and the HEXTE range 18 – 60 keV when modeling the spectra.

Three long observations with PCA exposure time $>$ 20 ks are available in the RXTE archive, along with hundreds of shorter monitoring observations. We combined the individual pointings of each observation as described in the RXTE Cookbook. The three long observations, LO1, LO2, and LO3, were kept separate, while the rest of the data between these observations were combined into “Data Sections” (DS1, DS2, and DS3). Data prior to LO1 were excluded to avoid spectral contamination from flaring events (see Reig et al. 2008 for a description of the flares). For DS3, we chose to use observations from the oscillating phase that had an average PCA 2 – 20 keV count rate of 10 counts s^{-1} PCU⁻¹ or higher. The observation identification numbers and other information are given in Table 1. The locations in time of LO1–3 are shown by the colored lines, and DS1–3 by the shaded regions, in Figure 1. The HEXTE data are very noisy, so we rebinned the counts at high energies using the *F*TOOL³ *grppha*. For LO1, we rebinned by 3 energy channels above 50 keV; for LO2, by 3 channels above 48 keV; and for LO3, by 4 channels above 35 keV. We did not rebin any counts in DS1. The HEXTE data of DS2–3 were so noisy we decided not to use them, as they might skew our spectral fits.

We have used XSPEC11⁴ models (Arnaud 1996, Dorman, B. & Arnaud, K. A. 2001) for all spectral fitting.

3. SPECTRAL ANALYSIS

3.1. Spectral Models

Our first step in spectral fitting was to choose an appropriate continuum model. We experimented with differ-

¹ See <http://heasarc.gsfc.nasa.gov/docs/xte/whatsnew/big.html> for more detailed information.

² The RXTE Cookbook is found at http://heasarc.gsfc.nasa.gov/docs/xte/recipes/cook_book.html.

³ *F*TOOLS descriptions and software can be found at http://heasarc/docs/software/ftools/ftools_menu.html.

⁴ The manual is found at <http://heasarc.nasa.gov/docs/xanadu/xspec/xspec11>.

ent models using the longest of all the observations, LO3, with total PCA exposure time ~ 27 ks.

The first continuum we tried is the standard XSPEC model cutoffpl, a power law with a high-energy exponential rolloff, with analytical form

$$C(E) = \alpha E^{-\Gamma} e^{-E/E_{\text{fold}}} \quad (1)$$

where α is the power law normalization, or number of photons $\text{keV}^{-1} \text{cm}^{-2} \text{s}^{-1}$ at 1 keV, Γ is the power law photon index, and E_{fold} is the e-folding energy of the exponential rolloff. This model is simple and used often, but can create an artificial linelike feature near E_{fold} due to a discontinuity at that energy (Coburn et al. 2002 and references therein). For this reason we compared cutoffpl with the following models to ensure the residuals agreed.

The second model we used is very similar to cutoffpl; we simply multiplied a power law (powerlaw in XSPEC) by a high-energy cutoff (highecut in XSPEC):

$$C(E) = \alpha E^{-\Gamma} \begin{cases} 1, & E \leq E_{\text{cut}} \\ \exp|-(E_{\text{cut}} - E)/E_{\text{fold}}|, & E > E_{\text{cut}} \end{cases} \quad (2)$$

Here E_{cut} is the cutoff energy and E_{fold} the e-folding energy.

We next fit the spectrum with a Fermi-Dirac cutoff (FDCO) from Tanaka (1986),

$$C(E) = \alpha E^{-\Gamma} \left[\exp\left(\frac{E - E_{\text{cut}}}{E_{\text{fold}}}\right) + 1 \right]^{-1} \quad (3)$$

This model has a smooth, continuous turnover. E_{cut} and E_{fold} are again the cutoff and e-folding energies in keV, but are not comparable to the parameters in cutoffpl or power \times highecut due to differences in the continua.

The final model we used is the Negative Positive Exponential (NPEX) model from Mihara (1995), which consists of two power laws with an exponential cut-off:

$$C(E) = (\alpha_1 E^{-\Gamma_1} + \alpha_2 E^{+\Gamma_2}) \times \exp\left(-\frac{E}{E_{\text{fold}}}\right) \quad (4)$$

where $\Gamma_1, \Gamma_2 > 0$ are the spectral indices of the two power laws, and α_1 and α_2 are their normalizations.

Each fit requires a Gaussian emission line at 6.4 keV, and some combination of a Gaussian emission line near 13 keV and an absorption feature near 10 keV. We find that in this case these different models produce fits of the same quality, as well as identical results, within the errors, for all comparable parameters, most notably the 10 keV absorption feature.

We chose to use cutoffpl, as it is the simplest model and in this case results in residuals that are nearly identical to those from the other models listed. Also, it is well suited for comparisons with many earlier results for similar sources, as in Coburn et al. (2002), and more recently, A 0535+26 (Caballero et al. 2008) and V 0332+53 (Mowlavi et al. 2006). The baseline model includes photoelectric absorption (phabs in XSPEC) and a Gaussian 6.4 keV emission line (gauss), so the final continuum model is

$$C(E) = e^{-N_{\text{H}}\sigma_{\text{bf}}(E)} \times \left\{ \alpha E^{-\Gamma} e^{-\frac{E}{E_{\text{fold}}}} + \beta \frac{1}{\sigma_{\text{Fe}}\sqrt{2\pi}} e^{-\frac{1}{2}[(E-E_{\text{Fe}})^2/\sigma_{\text{Fe}}^2]} \right\} \quad (5)$$

N_{H} and σ_{bf} are the absorption model components, and are respectively the hydrogen column density per H atom for material of cosmic abundance and the bound-free photoelectric absorption cross-section. The second term in the addition is the Gaussian emission line, in which β is its normalization (photons $\text{cm}^{-2} \text{s}^{-1}$), E_{Fe} (keV) is the iron emission line energy, and σ_{Fe} (keV) is the emission line width. This model is applied concurrently to the PCA and HEXTE data, differing only by a constant factor (the HEXTE spectrum is calibrated to ~ 0.8 times that of the PCA). For each spectral fit, we adjust the background strength to within $\sim 0.1\%$ using the command `recnorm` in XSPEC.

3.2. Detection of a 10 keV CRSF

The longest observation of SwiftJ1626.6–5156, LO3, was taken on 2006 January 31, during the post-outburst decay (see Figure 1). The first PCA pointing is ~ 21 ks long, and is followed immediately by a shorter pointing of ~ 6 ks. We have combined them to form a single spectrum with PCA integration time ~ 27 ks. The corresponding HEXTE observation has ~ 7.6 ks of integration time.

The phase-averaged spectrum of LO3 is shown in Figure 2. Panel (a) shows the residuals from fitting only with an absorbed cut-off power law, and panel (b) shows the fit with our continuum model from equation (6). The residuals from this model show an absorption feature near 10 keV and/or an emission feature near 14 keV. We first treat the feature as absorption only. We fit the feature with a Gaussian optical depth absorption line (gabs in XSPEC), which flattens the residuals in panel (c). Applying the $\Delta\chi^2$ -confidence test, we find the absorption-like feature at 9.7 keV to be clearly significant ($\gg 99.99\%$). We realize the F -test is technically not applicable (Protassov et al. 2002), but in this case the detection is so highly significant that more elaborate methods are not necessary.

The residuals in panel (b) could possibly be due to an emission feature near 14 keV, rather than absorption near 10 keV. Broad emission features in this energy range are often necessary to describe the spectra of HMXBs (Coburn et al. 2002, §6.4). Suchy et al. (2008) discuss a broad emission component at ~ 13 keV of unknown origin in Cen X-3; if such a feature also exists in our spectrum, it could potentially cause a negative residual near 10 keV. We therefore altered our fit by adding a broad emission line near 14 keV to the model. We find that an absorption feature at 9.7 keV is still required to remove residuals from the fit. A final fit with both the absorption and emission features (as in panel (c), only with an additional Gaussian emission line at 14 keV) yields $\chi^2/N_{\text{dof}} = 49.96/53 (= 0.94)$, as opposed to $52.76/56 (= 0.94)$. The fits are equally good.

We interpret the 10 keV absorption feature as a cyclotron resonance scattering feature (CRSF), or cyclotron line. We choose our best fit to be the simpler

of the two described above – our continuum model with a statistically significant absorption feature at 9.7 keV. Our best fit model $M(E)$ is therefore an absorbed cut-off power law plus a Gaussian emission line at ~ 6.4 keV, multiplied by a Gaussian optical depth absorption line at ~ 10 keV (phabs \times (cutoffpl + gauss) \times gabs):

$$M(E) = e^{-N_{\text{H}}\sigma_{\text{bf}}(E)} \times \left[\alpha E^{-\Gamma} e^{-E/E_{\text{fold}}} + \beta \frac{1}{\sigma_{\text{Fe}}\sqrt{2\pi}} e^{-(E-E_{\text{Fe}})^2/2\sigma_{\text{Fe}}^2} \right] \times \exp \left\{ - \left(\frac{\tau}{\sigma_{\text{cyc}}\sqrt{2\pi}} \right) e^{-\frac{1}{2}[(E-E_{\text{cyc}})/\sigma_{\text{cyc}}]^2} \right\} \quad (6)$$

Here τ , σ_{cyc} , and E_{cyc} are respectively the optical depth, line width, and line energy of the cyclotron line. The best-fit parameters for the LO3 spectrum, along with the iron line equivalent width and other characteristics, can be found in the third column of Table 2. The profile of the cyclotron line is shown in red in Figure 3.

Returning to Figure 2c, we note a small depression near 18 keV. In panel (d), we have fit this feature with another Gaussian optical depth absorption line with centroid energy $18.5_{-0.6}^{+0.9}$ keV, $\tau \sim 0.1_{-0.07}^{+0.09}$, and σ , which cannot be constrained, fixed at ~ 0.02 to minimize χ^2 . This additional component reduces χ^2 slightly, but it is clearly not significant here ($< 2\sigma$). We therefore do not include this feature in our best-fit model of the phase-averaged spectrum.

While we would not normally consider this a detection, we find that the addition of this 18 keV feature greatly improves the pulse phase-resolved spectral fits (see §3.4) and is likely the first harmonic of the fundamental CRSF. That this harmonic does not occur at twice the fundamental energy may be due in large part to the line energies, which shift with phase, being smeared by the phase-averaged spectrum. Other sources, for example V0332+53 (Pottschmidt et al. 2005, Kreykenbohm et al. 2005) and 4U 0115+63 (Heindl et al. 1999, Santangelo et al. 1999, Nakajima et al. 2006), have displayed cyclotron lines at non-integer multiples of the fundamental. Also, spacing that is not quite harmonic is expected when general relativistic effects are taken into account (Mészáros 1992), although such effects lead to wider rather than narrower energy spacings between the lines.

3.3. Confirming the 10 keV CRSF

Bumps or wiggles in the spectra of accreting X-ray pulsars are common, and have been discussed at some length by Coburn et al. (2002). They find residuals in the data/model ratio at the $\sim 0.8\%$ level in all the accreting systems they examine. These residuals could easily be interpreted as cyclotron features. There have been marginal detections of absorption features, possibly cyclotron lines, near 10 keV in other sources. One example is the recent work on XMMU J054134.7-682550 by Inam et al. (2008). These authors see what may be an absorption feature at 10 keV, but the count rate is too low to claim a significant detection. It is therefore unclear whether the line they detect is real, or if it is due to calibration uncertainty. For this reason, we must take extreme care to ensure that the feature we see is truly a cyclotron line and not a calibration uncertainty. (The

best PCA calibration is accurate to $\sim 1\%$ in the ratio between the data and model, Jahoda et al. 2006.)

To check that the 10 keV feature is consistent with a CRSF, we compared the Gaussian absorption model gabs with the cyclotron resonance scattering model cyclabs in XSPEC. We find similar centroid energies for the absorption feature using either model, and choose to use gabs in our analysis because its energy parameter gives a more accurate line energy value (the energy parameter of cyclabs, which has a Lorentzian optical depth profile, does not reflect the energy where the spectrum has a true minimum).

Using data only from PCU 2, which is the best calibrated of the five PCUs (Jahoda et al. 2006) and is most often turned on during observations, we compared the Swift J1626.6–5156 spectrum with a spectrum of the Crab pulsar and nebula composed of data taken between November 2005 – March 2006. This is the same time period during which the Swift J1626.6–5156 observations LO1–3 were taken. We were looking for an absorption-like feature near 10 keV. The Crab has no CRSFs, so if the feature were seen in the Crab spectrum, we would know that the Swift J1626.6–5156 feature was instrumental in origin. We modeled the Crab spectrum with an absorbed power law, freezing N_{H} at $4 \times 10^{21} \text{ cm}^{-2}$, as quoted by Weisskopf et al. (2004). The power law parameters were left free, and we found that $\Gamma = 2.095$ with a normalization of 10.343 gave the best fit. The data/model ratio is ~ 0.99 near 10 keV. This is a $\sim 1\%$ deviation from a perfect ratio of unity, which is expected due to calibration uncertainties – no absorption feature is found at 10 keV in the Crab spectrum. We repeated the procedure with PCU 2 data from LO3, using a cut-off power law and freezing N_{H} and Γ to the values in Table 2. In this case, the ratio near 10 keV is ~ 0.91 , a much larger residual than one due to calibration errors.

We next took a model- and calibration-independent approach by comparing the raw counts in each spectral channel of Swift J1626.6–5156 with those of the Crab. Our procedure is similar to that used in Figure 3 of Orlandini et al. (1998). We first removed the background counts from each raw spectrum, being sure to account for the difference in exposure time between the two sources. We next adjusted the Crab count rate such that the Crab and Swift J1626.6–5156 would have the same broad band shape underlying any possible line features:

$$R_{\text{Crab}}^{\text{new}}(E) = R_{\text{Crab}}^{\text{raw}}(E) E^{(\Gamma_{1626} - \Gamma_{\text{Crab}})} e^{-E/E_{\text{fold}}} \quad (7)$$

where R is the count rate at each spectral energy; $R_{\text{Crab}}^{\text{raw}}$ is the raw Crab spectrum, and $R_{\text{Crab}}^{\text{new}}$ is the adjusted Crab spectrum, calculated by forcing the spectral index of the Crab and Swift J1626.6–5156 to be the same. We have accounted for the cut-off power law in the spectrum of Swift J1626.6–5156 by including the factor of $e^{-E/E_{\text{fold}}}$. We then divide the Swift J1626.6–5156 count rates by those of the Crab and plot the resulting spectrum, which is flat except for residuals due to contrasting features between the two sources' spectra. The spectral indices that yield a flat continuum after applying equation (7) are $\Gamma_{1626} = 1.59$ and $\Gamma_{\text{Crab}} = 2.05$. In the residuals are an enhancement at 6.4 keV due to the iron line in Swift J1626.6–5156 and a depression at ~ 10 keV, rather than a smooth transition between the iron line and the power

law tail. This confirms, independent of the response function or spectral model, that the absorption feature does not result from a calibration error and is instead a real spectral feature. We therefore believe that the feature at 10 keV is a real feature in the source spectrum caused by cyclotron resonance scattering.

3.4. Pulse Phase-Resolved Spectra

We again used LO3 for our phase-resolved spectral analysis. We extracted Good Xenon event data with time resolution 3.9 ms and corrected the event times to the barycenter. A pulse search on these data resulted in a pulse period of 15.3582 s, on which we folded to obtain a pulse profile. We are using a different observation than Reig et al. (2008), and therefore accept the difference between our measured period and their period of 15.3718 s, and we note that the neutron star has apparently spun up since the beginning of the outburst when their data were taken.

As discussed by Reig et al. (2008; Figure 3), the pulse profile shows a single broad peak with a roughly constant maximum over 4 phase bins. The falling edge seems to be steeper than the rising edge, which may be an artifact from the period folding. We did not include a binary correction due to insufficient information about the orbit.

We divided the pulse profile into 16 phase bins for spectral analysis and used IKFASEBIN⁵ to extract spectra at each phase. Each spectrum was fit using equation (6) with an additional edge component at 5 keV to account for the Xenon L-edge calibration feature (Jahoda et al. 2006, §3.1). We found it necessary to remove one spectral bin at ≈ 4.5 keV (spectral bin 12) from each phase's spectrum to improve the overall fit. We assume that the uncertainty in this spectral bin is due to calibration at lower energies and has no physical significance for the model. The column density and the iron emission energy were frozen at $3.4 \times 10^{22} \text{ cm}^{-2}$ and 6.4 keV, respectively. To better constrain the spectral index, the folding energy of the cut-off power law was also frozen at 10.98 keV.

Using only the continuum model on the phase-resolved spectra led to unacceptable fits (column $\chi_{\text{red},0}^2$ in Table 3) throughout the whole pulse. Including a CRSF in the form of a Gaussian optical depth absorption line at ≈ 10 keV improves the fits significantly, but does not result in a sufficiently low χ^2 during the maximum of the main peak. Including a second absorption line in these 4 phase bins improved the fits to acceptable values. These phase bins are shown by the shaded region of Figure 4. The width of the second line was frozen at 2.5 keV to better constrain the other parameters (see column $\chi_{\text{red},2}^2$). The centroid energy is roughly twice the energy of the fundamental line, and is probably the first harmonic line mentioned in the discussion of the phase-averaged spectrum in Figure 2 (§3.2).

Figure 4 shows the free continuum and fundamental CRSF parameters throughout the pulse phase. The power law index decreases (hardens) throughout the peak, and increases (softens) in the minimum. The power law normalization follows as expected throughout the pulse profile, reaching $\sim 0.18 \text{ photons cm}^{-2} \text{ keV}^{-1}$ throughout the peak. The CRSF energy shows a small

increase during the rising edge, and a drastic increase of more than 20% at the beginning of the falling edge. Strong variations in the CRSF centroid energy have also been observed in other sources, e.g. Cen X-3 (Suchy et al. 2008 and references therein) and Vela X-1 (La Barbera et al. 2003, Kreykenbohm et al. 2002). The width and depth of the scattering feature are mostly constant throughout the pulse, with a small dip in the rising edge.

3.5. Persistence of Spectral Features

Thus far we have only discussed LO3, the longest of the three observations. The CRSF is detected in the first two observations as well. Figure 3 shows the shape of the line in each case. The $\lesssim 2\sigma$ harmonic is present in the spectra of LO2 and LO3 (green and red). We also detect a strong iron line in each of the three spectra. The best-fit spectral parameters for each of the three long observations are shown in Table 2.

One question we may ask is whether or not the cyclotron line persists throughout and beyond the outburst decay. To answer this, we combined sections of data into single spectra to search for the line. The data selection is described in §2 and outlined in Table 1.

Both the iron line and the CRSF were present throughout the outburst of Swift J1626.6–5156; they are detected in each long observation and each Data Section. Interestingly, we find that the spectrum from the oscillatory stage of the light curve (DS3) is best fit by the addition of a Gaussian emission line at ~ 15 keV, a component that was not necessary in any of the spectra taken during the outburst decay but that is commonly used to fit HMXB spectra (Coburn et al. 2002). All fit parameters are given in Table 2. The values of E_{cyc} are suggestive of an evolution of the cyclotron line energy with luminosity, which will be discussed further below.

4. DISCUSSION

We find evidence for a 6.4 keV Fe K emission line and cyclotron resonance scattering features at ~ 10 and 20 keV in the spectrum of the Be/X-ray binary Swift J1626.6–5156. While the harmonic CRSF is not seen at a significant level in the phase-averaged spectrum, pulse phase-resolved spectroscopy shows it is a necessary addition to the spectral fit between phases $\sim 0.4 - 0.7$.

The source is in the galactic plane, so the diffuse Galactic Fe K emission must at least contribute to our measured iron line flux. For a typical Galactic ridge field, the total Fe K line flux is $\sim 3.8 \times 10^{-4} \text{ photons s}^{-1} \text{ cm}^{-2} \text{ deg}^{-2}$ (Ebisawa et al. 2008). The PCA solid opening angle is 0.975 deg^2 and the effective area of 1 PCU at 6.4 keV is 1000 cm^2 , so the diffuse Fe K line flux (averaged over the area) seen by the PCA is $\sim 0.37 \text{ photon s}^{-1}$ (Jahoda et al. 2006). We calculated the 2.6–20 keV Fe K line flux from each of the three long observations by first finding the flux of the best-fit model and then removing the emission line and, without refitting, calculating the flux again. We find Fe K fluxes of $\sim 3 \text{ photons s}^{-1}$ from LO1, $\sim 2.7 \text{ photons s}^{-1}$ from LO2, and $\sim 1 \text{ photon s}^{-1}$ from LO3, indicating that most of the iron line emission is coming from Swift J1626.6–5156.

We can use the cyclotron line energy to estimate the strength of the magnetic field near the polar emitting region. The fundamental and subsequent harmonic cyclotron line energies are related to the local magnetic

⁵ For usage, see <http://pulsar.sternwarte.uni-erlangen.de/wilms/research/analysis/rxte/pulse.html>

field strength by

$$E_n = m_e c^2 \frac{\sqrt{1+2n(B/B_{\text{crit}})\sin^2\theta}-1}}{\sin^2\theta} \frac{1}{1+z} \quad (8)$$

$$\approx n(11.6 \text{ keV})(1+z)^{-1} B_{12}$$

(Mészáros 1992) where m_e is the electron rest mass, $n = (1, 2, 3, \dots)$ is the integer harmonic number, $B_{\text{crit}} \sim 4 \times 10^{13} \text{ G}$ is the critical field strength for resonant scattering, and θ is the angle between the photon direction and the magnetic field vector; z is the gravitational redshift at the neutron star surface ($z \sim 0.3$ for a neutron star with mass $1.4 M_\odot$ and radius $\sim 10^6 \text{ cm}$) and $B_{12} = B/(10^{12} \text{ G})$. A fundamental energy of $\sim 10 \text{ keV}$ therefore implies the magnetic field local to the neutron star's hot spot is $\sim 8.6(1+z) \times 10^{11} \text{ G} \sim 1.1 \times 10^{12} \text{ G}$.

As a consistency check, we estimate the global magnetic field strength, assuming that the neutron star has reached its equilibrium spin rate through interplay between an accretion disk and the magnetic field. We refer to Ghosh & Lamb (1979) and Shapiro & Teukolsky (1983, Ch. 15) for our calculation, and use the CRSF energy and pulse period of LO3 for the comparison.

To be sure that the discovery outburst did not significantly change its spin rate, thus throwing it out of equilibrium, we referred to Figure 1 of Finger et al. (1996), which shows the spin period changing with time during the largest outburst seen from the HMXB A0535+262. This caused a 0.1–0.2% change in the pulsar's spin period. We can safely assume that the period of Swift J1626.6–5156 will not change by a larger percentage than this, so the small change in P_{spin} will have little effect on our estimate of the global magnetic field.

We estimate B_{global} by equating the Alfvén radius r_A with the corotation radius, at which the orbital velocity is equivalent to the surface velocity of the rotating star, thus giving $\omega_{\text{spin}} \approx \sqrt{GM/r_A^3} \text{ rad s}^{-1}$, where

$$r_A \approx 3.2 \times 10^8 \dot{M}_{17}^{-2/7} \mu_{30}^{4/7} \left(\frac{M}{M_\odot} \right)^{-1/7} \text{ cm} \quad (9)$$

Here $\dot{M}_{17} = \dot{M}/(10^{17} \text{ g s}^{-1})$ is the mass accretion rate and $\mu_{30} = \mu/(10^{30} \text{ G cm}^3)$ is the dipolar magnetic moment. $P_{\text{spin}} = 15.3718 \text{ s}$ is our measured spin period, so $\omega_{\text{spin}} \sim 0.41 \text{ rad s}^{-1}$ and $r_A \sim 1 \times 10^9 \text{ cm}$. To estimate the average \dot{M} over the source's lifetime, we must first estimate the luminosity of the source outside of outburst. The direction of our source is toward the Galactic center, but its distance d is unknown, so we will calculate L and B for distances of 5 and 10 kpc. We next assume that the current low-luminosity state of the source is typical outside of outburst, and from the source's spectrum during this state (DeCesar et al. 2009) we derive a 2–60 keV flux of $2.9 \times 10^{-11} \text{ erg cm}^{-2} \text{ s}^{-1}$, giving a luminosity of $\sim 4.3 \times 10^{34} \text{ erg s}^{-1}$ at 5 kpc and $\sim 1.7 \times 10^{35} \text{ erg s}^{-1}$ at 10 kpc for isotropic emission. The mass accretion rate, for an efficiency $\eta \approx 0.1$, is then $\dot{M} = L/(\eta c^2) \sim 5 \times 10^{14} \text{ g s}^{-1}$ ($d = 5 \text{ kpc}$) or $\sim 2 \times 10^{15} \text{ g s}^{-1}$ ($d = 10 \text{ kpc}$). Using equation (9), we find $\mu_{30} \sim 0.5 \text{ G cm}^3$ ($d = 5 \text{ kpc}$) or $\sim 1 \text{ G cm}^3$ ($d = 10 \text{ kpc}$). The global dipolar magnetic field strength is then

$$B_{\text{global}} = 2\mu/R_{\text{NS}}^3 = \begin{cases} 1 \times 10^{12} \text{ G}, & d = 5 \text{ kpc} \\ 2 \times 10^{12} \text{ G}, & d = 10 \text{ kpc} \end{cases} \quad (10)$$

This is consistent with the field strength derived from the cyclotron line, which for LO3 with a CRSF energy of $\sim 9.7 \text{ keV}$ is $B \sim 1 \times 10^{12} \text{ G}$.

Something else to consider is the relationship between the cyclotron line energy and the source's X-ray luminosity. Her X-1 is an example of a system containing an accreting magnetized NS whose cyclotron line energy is positively correlated with luminosity (Staubert et al. 2007). In contrast to this are V0332+53 (Tsygankov et al. 2006) and 4U 0115+63 (Nakajima et al. 2006), in which the cyclotron line energy decreases as the source brightens. It was suggested by Staubert et al. (2007) that a positive correlation between E_{cyc} and luminosity would occur for systems accreting at a sub-Eddington rate, while the negative correlation would occur when the accretion is locally super-Eddington. They show that the fractional change in E_{cyc} is directly proportional to the fractional change in L . If such a relationship can be confirmed with cyclotron line sources of known distances, it may be possible to use observations of cyclotron lines as standard candles.

The 90% errors on the cyclotron line energy in Table 2 point to a possible correlation between E_{cyc} and luminosity. We calculated the 3σ errors on the line energy of LO1, LO3, and DS3, and find that the energies are not consistent with each other within the errors. The 3σ confidence range on the CRSF energy is 10.15–10.55 keV during LO1; 9.58–9.85 keV during LO3; and 9.32–9.56 keV during DS3. The measured decrease in the line energy with decreasing flux (luminosity) is indicative of a positive correlation between E_{cyc} and L and is apparent at the 99.7% confidence level in our data. Further observations in a future outburst are necessary to confirm this correlation. We note that N_{H} in Table 2 decreases over the time of the outburst as well. Since $L \propto \dot{M}$, and \dot{M} depends on the amount of material in the system, the decreasing values of N_{H} may reflect the diminishment of material from the neutron star's surroundings.

5. CONCLUSION

We have clearly detected a spectral feature at $\sim 10 \text{ keV}$ in the spectrum of the Be/X-ray binary Swift J1626.6–5156. Every aspect of our analysis points to this feature being a cyclotron resonance scattering feature. The second harmonic of the CRSF, at an energy of $\sim 18 \text{ keV}$, is seen between pulse phases 0.4–0.7. The fundamental cyclotron line and the $\sim 6.4 \text{ keV}$ iron emission line persist throughout the source's outburst and oscillatory stages.

The neutron star's magnetic field strength of $\sim 10^{12} \text{ G}$, derived from the cyclotron line energy, is physically realistic and typical of high-mass X-ray binaries. We find that this field strength is consistent with the scenario of spin equilibration via disk accretion, and we do not rule out the possibility that Swift J1626.6–5156 may host an accretion disk.

Comparing the 3σ confidence intervals of the fundamental CRSF energies in LO1, LO3, and DS3 reveals a positive correlation between the line energy and the source luminosity. This behavior is similar to that of Her X-1, in which the luminosity and line energy are also positively correlated, and according to the model of Staubert et al. (2007) implies the outburst of Swift

J1626.6–5156 was sub-Eddington. Observations during future outbursts of Swift J1626.6–5156 will be beneficial in confirming this relationship between its luminosity and cyclotron line energy.

We thank Wayne Coburn for pointing out Swift J1626.6–5156 as a candidate cyclotron line source. This work was funded under solicitation NNH07ZDA001N-

SWIFT4 of the Swift Guest Investigator program and NSF Grant AST0708424. J. Wilms acknowledges partial funding from the Bundesministerium für Wirtschaft und Technologie through Deutsches Zentrum für Luft- und Raumfahrt grants 50 OR 0808 and 50 OR 0905. S. Suchy acknowledges the support of NASA contract NAS5-30720 and NASA grant NNX08AZ82G.

REFERENCES

- Arnaud, K. A. 1996, *Astronomical Data Analysis Software and Systems V*, eds. Jacoby, G. and Barnes, J., p17, ASP Conf. Series volume 101
- Caballero, I., Santangelo, A., Kretschmar, P., Staubert, R., Postnov, K., Klochkov, D., Camero-Arranz, A., Finger, M. H., Kreykenbohm, I., Pottschmidt, K., Rothschild, R. E., Suchy, S., Wilms, J., & Wilson, C. A. 2008, *A&A* 480, 17
- Coburn, W., Heindl, W. A., Rothschild, R. E., Gruber, D. E., Kreykenbohm, I., Wilms, J., Kretschmar, P., & Staubert, R. 2002, *ApJ*, 580, 394
- Coburn, W., Kretschmar, P., Kreykenbohm, I., McBridge, V. A., Rothschild, R. E., Staubert, R., & Wilms, J. 2006, *Advances in Space Research* (New York, NY: ScienceDirect, Elsevier Science), vol. 38, 12, p. 2747
- Coe, M. J. 2000, *ASP Conf. Series*, 214, 656
- DeCesar, M. E., Pottschmidt, K., Wilms, J. 2009, *ATel* 2036
- Dorman, B. & Arnaud, K. A. 2001, *Astronomical Data Analysis Software and Systems X* eds. F.R. Harnden, Jr., F.A. Primini, and H.E. Payne, vol. 238, p. 415
- Ebisawa, K., Yamauchi, S., Tanaka, Y., Koyama, K., Ezoe, Y., Bamba, A., Kokubun, M., Hyodo, Y., Tsujimoto, M., & Takahashi, H. 2008, *PASJ*, 60, 223
- Finger, M. H., Wilson, R. B., & Harmon, B. A. 1996, *ApJ*, 459, 288
- Gerend, D. & Boynton, P. E. 1976, *ApJ*, 209, 562
- Ghosh, P. & Lamb, F. K. 1979, *ApJ*, 232, 259
- Heindl, W. A., Coburn, W., Gruber, D. E., Pelling, M. R., Rothschild, R. E., Wilms, J., Pottschmidt, K., & Staubert, R. 1999, *ApJ*, 521, 49
- Heindl, W. A., Rothschild, R. E., Coburn, W., Staubert, R., Wilms, J., Kreykenbohm, I., & Kretschmar, P. 2004, *AIP Conf. Proc.*, 714, 323
- Inam, S. C., Townsend, L. J., McBride, V. A., Baykal, A., Coe, M. J., & Corbet, R. H. D. 2009, *MNRAS*, 395, 1662
- Jahoda, K., Markwardt, C. B., Radeva, Y., Rots, A. H., Stark, M. J., Swank, J. H., Strohmayer, T., Zhang, W., & Morgan, E. H. 2006, *ApJS*, 163, 401
- Kreykenbohm, I., Coburn, W., Wilms, J., Kretschmar, P., Staubert, R., Heindl, W. A., & Rothschild, R. E. 2002, *A&A*, 395, 129
- Kreykenbohm, I., Mowlavi, N., Produit, N., Soldi, S., Walter, R., Dubath, P., Lubiński, P., Türler, M., Coburn, W., Santangelo, A., Rothschild, R. E., & Staubert, R. 2005, *A&A*, 433, 45
- Krimm, H., Barthelmy, S., Capalbi, M., Gehrels, N., Gronwall, C., & Palmer, D. 2005, *GCN* 4361
- La Barbera, A., Santangelo, A., Orlandini, M., & Segreto, A. 2003, *A&A*, 400, 993
- Lomb, N. R. 1976, *Ap&SS*, 39, 447
- Lutovinov, A. & Tsygankov, S. 2008, *AIP Conf. Proc.*, 1054, 191
- Markwardt, C. B. & Swank, J. H. 2005, *ATel* 679
- Mészáros, P. 1992, *High-Energy Radiation from Magnetized Neutron Stars* (Chicago: Univ. Chicago Press)
- Mihara, T., 1995, Ph.D. thesis, RIKEN, Tokio
- Mowlavi, N., Kreykenbohm, I., Shaw, S. E., Pottschmidt, K., Wilms, J., Rodriguez, J., Produit, N., Soldi, S., Larsson, S., & Dubath, P. 2006, *A&A* 451, 187
- Nakajima, M., Mihara, T., Makishima, K., & Niko, H. 2006, *ApJ*, 646, 1125
- Negueruela, I. & Marco, A. 2006, *ATel* 739
- Orlandini, M., dal Fiume, D., Frontera, F., Cusumano, G., del Sordo, S., Giarrusso, S., Piraino, S., Segreto, A., Guainazzi, M., & Piro, L. 1998, *A&A*, 332, 121
- Palmer, D., Barthelmy, S., Cummings, J., Gehrels, N., Kennea, J., Krimm, H., Markwardt, C. B., & Tueller, J. 2005, *ATel* 678
- Pottschmidt, K., Kreykenbohm, I., Wilms, J., Coburn, W., Rothschild, R. E., Kretschmar, P., McBride, V., Suchy, S., & Staubert, R. 2005 *ApJ*, 634, 97
- Priedhorsky, W. C. & Holt, S. S. 1987, *Space Science Reviews*, 45, 291
- Protassov, R., van Dyk, D. A., Connors, A., Kashyap, V. L., Siemiginowska, A. 2002, *ApJ*, 571, 545
- Reig, P., Belloni, T., Israel, G. L., Campana, S., Gehrels, N., & Homan, J. 2008 *A&A*, 485, 797
- Rothschild, R. E., Blanco, P. R., Gruber, D. E., Heindl, W. A., MacDonald, D. R., Marsden, D. C., Pelling, M. R., Wayne, L. R., & Hink, P. L. 1998, *ApJ*, 496, 538
- Santangelo, A., Segreto, A., Giarrusso, S., dal Fiume, D., Orlandini, M., Parmar, A. N., Oosterbroek, T., Bulik, T., Mihara, T., Campana, S., Israel, G. L., & Stella, L. 1999 *ApJ*, 523, 85
- Scargle, J. D. 1982, *ApJ*, 263, 835
- Shapiro, S. L. & Teukolsky, S. A. 1983, *Black Holes, White Dwarfs, and Neutron Stars: The Physics of Compact Objects* (New York, NY: John Wiley & Sons)
- Staubert, R., Shakura, N. I., Postnov, K., Wilms, J.; Rothschild, R. E.; Coburn, W., Rodina, L., & Klochkov, D., 2007, *A&A*, 465, 25
- Suchy, S., Pottschmidt, K., Wilms, J., Kreykenbohm, I., Schoenherr, G., Kretschmar, P., McBride, V., Caballero, I., Rothschild, R. E., & Grinberg, V., 2008, *ApJ*, 675, 1487
- Tanaka, Y., 1986, In: Mihalas D., Winkler, K. H. (eds.) *Radiation Hydrodynamics in stars and compact objects*. Springer, New York, Heidelberg, p. 198
- Trowbridge, S., Nowak, M. A., & Wilms, J. 2007, *ApJ*, 670, 624
- Tsygankov, S. S., Lutovinov, A. A., Churazov, E. M., & Sunyaev, R. A. 2006, *MNRAS*, 371, 19
- Weisskopf, M. C., O’Dell, S. L., Paerels, F., Elsner, R. F., Becker, W., Tennant, A. F., & Swartz, D. A. 2004, *ApJ*, 601, 1050
- Wilms, J., Nowak, M. A., Pottschmidt, K., Pooley, G. G., Fritz, S. 2006, *A&A*, 447, 245

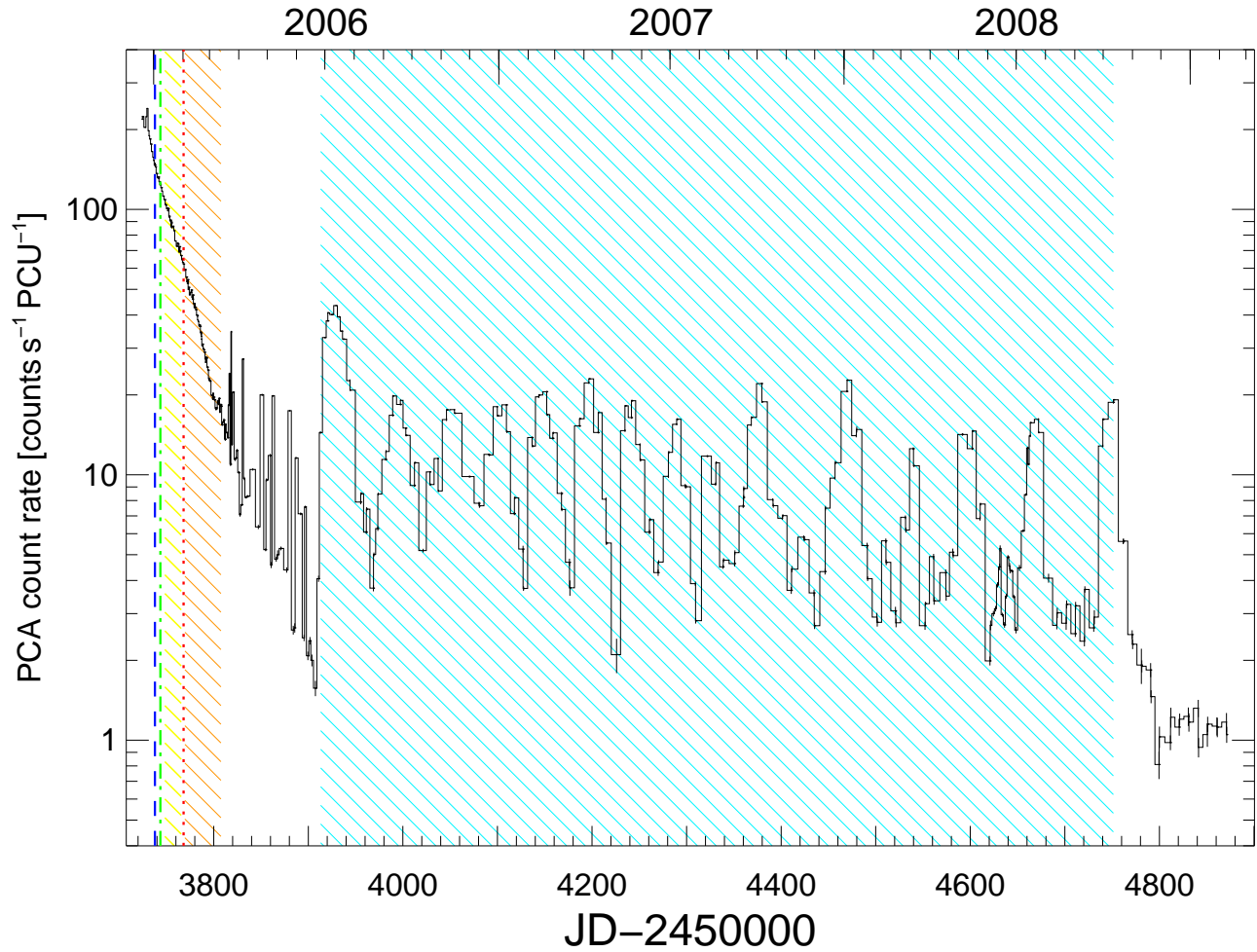


FIG. 1.— PCA light curve of Swift J1626.6–5156, taken from HEASARC’s RXTE mission-long data archive (<ftp://legacy.gsfc.nasa.gov/xte/data/archive/MissionLongData>). It shows the background-subtracted 2 – 20 keV count rate as recorded in standard2 mode (16 s time resolution), averaged over each observation and normalized to a single PCU. The three vertical lines indicate when the longest observations were taken in January 2006. LO1 is the blue dashed line, LO2 the green dot-dashed line, and LO3 the red dotted line. The shaded regions represent the Data Sections, with DS1 in yellow (black in grayscale), DS2 in orange (gray in grayscale), and DS3 in teal (light gray in grayscale).

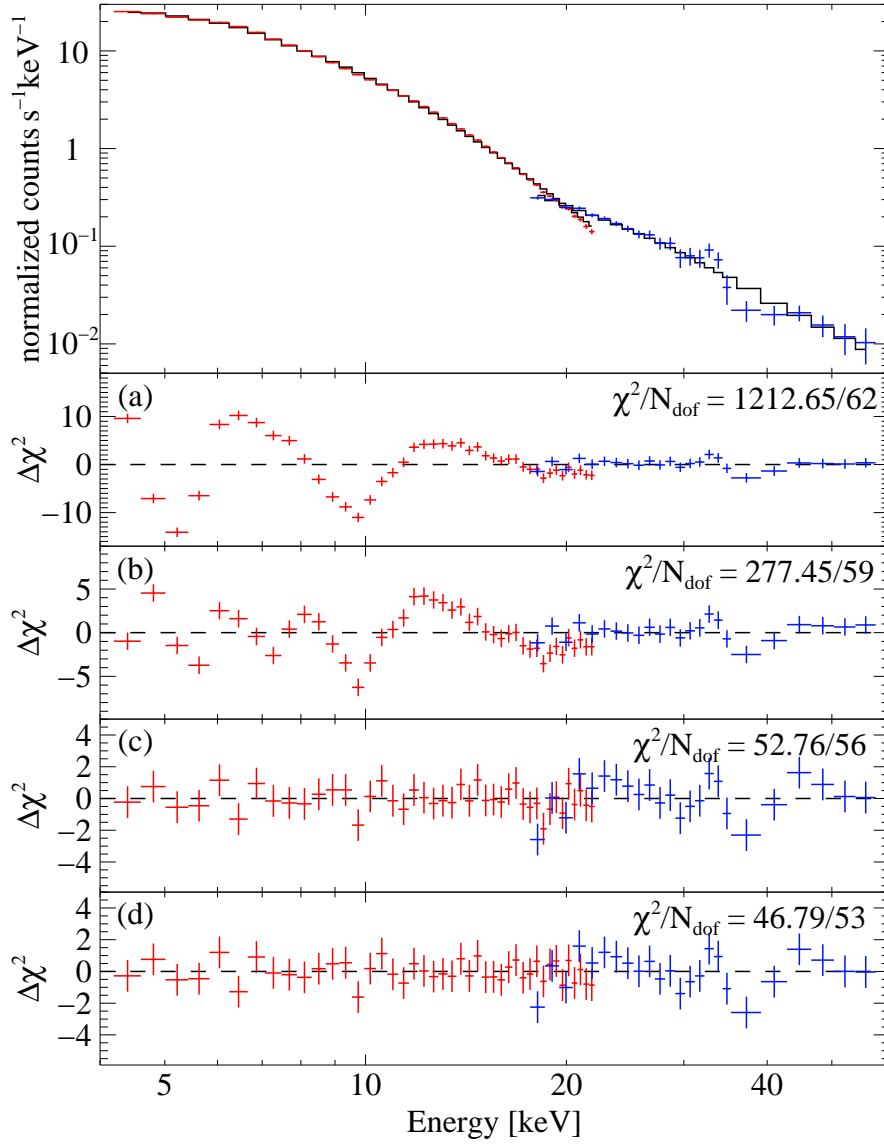


FIG. 2.— The 4.5 – 56 keV spectrum from LO3. PCA data are shown in red (dark gray in grayscale), HEXTE data in blue (light gray in grayscale). *a*) The $\Delta\chi^2$ residuals (delchi in XSPEC) left from fitting the spectrum with a cut-off power law. The spectrum peaks near 6.4 keV and dips near 10 keV. *b*) Residuals from adding a Gaussian emission line (gauss) at ~ 6.4 keV to the cut-off power law, completing our continuum fit from equation (6). The depression at 10 keV remains. *c*) Including a Gaussian optical depth absorption (gabs) line near 10 keV removes the absorption feature and greatly improves the model, giving our best fit (equation 6). There may be a second feature near 20 keV. *d*) A second Gaussian optical depth absorption feature included near 18 keV marginally improves the fit.

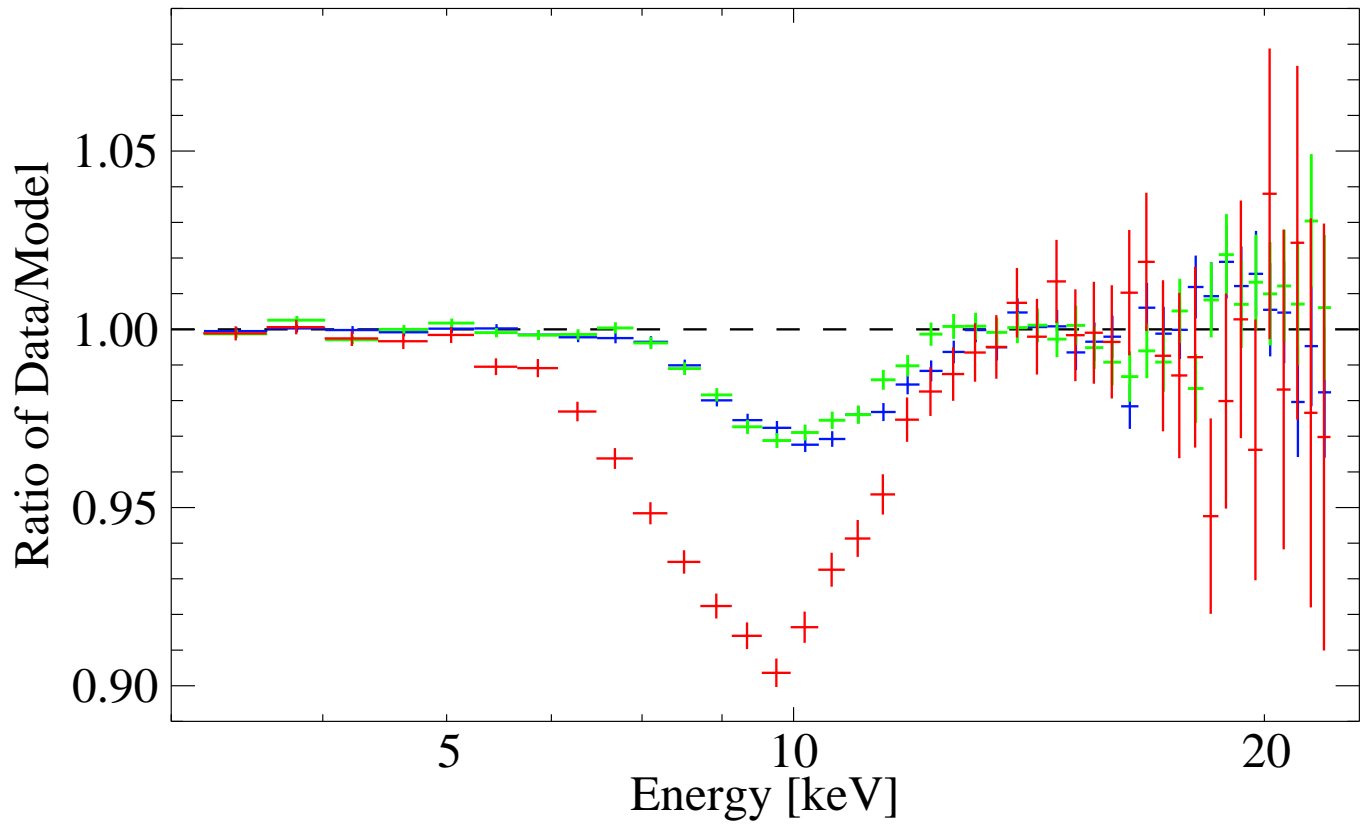


FIG. 3.— Removing the Gaussian optical depth absorption component in our spectral model reveals the shape of the fundamental cyclotron line at ~ 10 keV in LO1 (blue; light gray in grayscale), LO2 (green; gray in grayscale), and LO3 (red; dark gray in grayscale).

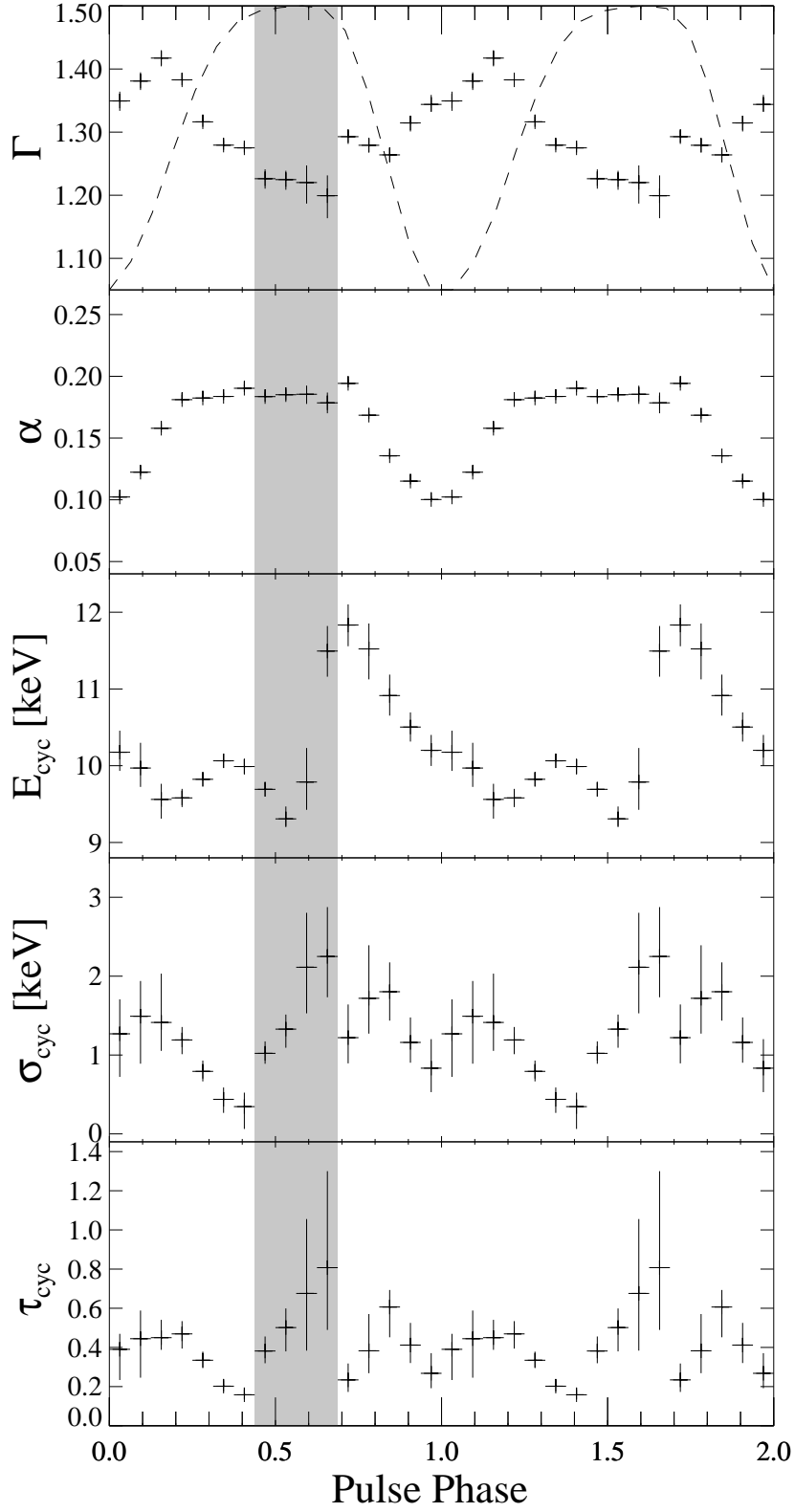


FIG. 4.— Variation of LO3 spectral parameters with phase. The shaded region indicates the 4 phase bins where a second line is necessary for an acceptable fit.

TABLE 1
OBSERVATION KEY

Name	Observation ID	Date	JD - 2450000	PCA t_{exp}	HEXTE t_{exp} [ks]
LO1	91081-13-01	2006 Jan 1	3736.05	26.4	8.4
LO2	91081-13-02	2006 Jan 6	3741.15	23.6	7.4
DS1	91082-01-01 - 91082-01-27	2006 Jan 12-30	3747.73-3765.10	23.3	7.1
LO3	91081-13-04	2006 Jan 31	3766.59	27.6	7.7
DS2	91082-01-32 - 91082-01-93	2006 Feb 1-Mar 13	3767.64-3807.52	51.2	-
DS3	92412-01-27 - 93402-01-48	2006 Jun 26-2008 Oct 10	3912.21-4750.82	78.8	-

TABLE 2
SPECTRAL PARAMETERS FOR PHASE AVERAGED SPECTRA

Name	N_{H} [10^{22}] ^b	Γ	α [10^{-1}] ^c	E_{fold} [keV]	E_{Fe} [keV]	σ_{Fe} [keV]	β [10^{-3}] ^d	E_{cyc} [keV]	σ_{cyc} [keV]	τ_{cyc}	F [10^{-10} cgs]	χ^2/N_{dof}
LO1	$4.8^{+0.6}_{-0.6}$	$1.11^{+0.04}_{-0.05}$	$2.8^{+0.2}_{-0.3}$	$10.46^{+0.33}_{-0.34}$	$6.33^{+0.03}_{-0.04}$	$0.49^{+0.05}_{-0.05}$	$3.3^{+0.5}_{-0.4}$	$10.23^{+0.09}_{-0.09}$	$0.99^{+0.17}_{-0.17}$	$0.097^{+0.025}_{-0.021}$	$19.10^{+0.02}_{-0.10}$	81.9/68
LO2	$4.5^{+0.8}_{-0.7}$	$1.20^{+0.06}_{-0.05}$	$2.5^{+0.3}_{-0.2}$	$11.50^{+0.52}_{-0.39}$	$6.30^{+0.04}_{-0.04}$	$0.54^{+0.07}_{-0.05}$	$3.0^{+0.4}_{-0.5}$	$10.01^{+0.09}_{-0.08}$	$0.76^{+0.15}_{-0.16}$	$0.082^{+0.020}_{-0.017}$	$16.80^{+0.03}_{-0.20}$	78.9/68
DS1	$4.8^{+0.8}_{-0.7}$	$1.37^{+0.07}_{-0.06}$	$2.4^{+0.3}_{-0.3}$	$12.72^{+0.79}_{-0.37}$	$6.34^{+0.05}_{-0.04}$	$0.45^{+0.06}_{-0.08}$	$1.7^{+0.3}_{-0.3}$	$9.74^{+0.07}_{-0.07}$	$0.96^{+0.13}_{-0.12}$	$0.15^{+0.02}_{-0.02}$	$11.80^{+0.04}_{-0.20}$	94.1/76
LO3	$3.4^{+0.7}_{-0.8}$	$1.32^{+0.09}_{-0.09}$	$1.7^{+0.2}_{-0.2}$	$10.98^{+0.97}_{-0.91}$	$6.38^{+0.04}_{-0.04}$	$0.19^{+0.10}_{-0.18}$	$0.9^{+0.2}_{-0.1}$	$9.71^{+0.07}_{-0.07}$	$1.27^{+0.16}_{-0.15}$	$0.33^{+0.04}_{-0.06}$	$8.62^{+0.04}_{-0.19}$	52.8/56
DS2	$1.4^{+0.8}_{-1.2}$	$1.61^{+0.07}_{-0.08}$	$1.0^{+0.1}_{-0.1}$	$19.07^{+1.83}_{-2.47}$	$6.36^{+0.03}_{-0.06}$	$0.41^{+0.05}_{-0.06}$	$0.8^{+0.2}_{-0.1}$	$10.00^{+0.08}_{-0.08}$	$0.64^{+0.02}_{-0.02}$	$0.25^{+0.04}_{-0.04}$	$4.44^{+0.03}_{-0.15}$	59.4/33
DS3 ^a	–	$1.37^{+0.07}_{-0.07}$	$0.33^{+0.02}_{-0.02}$	$13.20^{+1.67}_{-1.30}$	$6.48^{+0.02}_{-0.02}$	$0.41^{+0.05}_{-0.06}$	$0.40^{+0.04}_{-0.04}$	$9.44^{+0.07}_{-0.06}$	$0.64^{+0.11}_{-0.12}$	$0.25^{+0.04}_{-0.04}$	$2.06^{+0.003}_{-0.04}$	52.4/32

NOTE. — The best-fit spectral parameters from each observation or group of observations. N_{H} is the column density, Γ the power law photon index, α the power law normalization, E_{fold} the folding energy of the cut-off power law, E_{Fe} , σ_{Fe} , and β the iron emission line energy, width, and normalization, E_{cyc} , σ_{cyc} , and τ_{cyc} the energy, width, and optical depth of the Gaussian optical depth absorption line profile used to fit the cyclotron line, F the 2.64 – 20 keV source flux in units of 10^{-10} erg cm $^{-2}$ s $^{-1}$, and χ^2/N_{dof} the reduced χ^2 (where N_{dof} is the number of degrees of freedom), of each spectral fit. The changing N_{dof} results from differences in rebinning of the HEXTE data (see §2) for the LO1–LO3 columns, and from our choice to not use HEXTE data for DS2–3. The error bars quoted are at the 90% level. The 90% flux errors were calculated in XSPEC using 1000 draws from a Gaussian distribution. ^aDS3 requires an additional Gaussian emission component with energy $15.18^{+0.17}_{-0.17}$ keV, σ fixed at 0.30 keV, and normalization $7.3^{+1.4}_{-1.4} \times 10^{-5}$ total photons cm $^{-2}$ s $^{-1}$. ^bValues N_{H} are in units of 10^{22} atoms cm $^{-2}$. The origin of this emission line is unknown, but a similar component is commonly needed to fit spectra of HMXBs. It was unnecessary for the spectral fits of LO1 through DS2. ^cUnits are 10^{-1} photons keV $^{-1}$ cm $^{-2}$ s $^{-1}$ at 1 keV. ^dValues are given in units of 10^{-3} total photons cm $^{-2}$ s $^{-1}$.

TABLE 3
SPECTRAL PARAMETERS FOR PHASE RESOLVED SPECTRA FROM LO3

Phase Bin	Γ	α (10^{-1}) ^a	σ_{Fe} (keV)	β (10^{-3}) ^b	$E_{\text{cyc},1}$ (keV)	$\sigma_{\text{cyc},1}$ (keV)	$\tau_{\text{cyc},1}$	$E_{\text{cyc},2}$ (keV)	$\sigma_{\text{cyc},2}$ (keV)	$\tau_{\text{cyc},2}$	$\chi^2_{\text{red},2}$ 41 dof	$\chi^2_{\text{red},1}$ 43 dof	$\chi^2_{\text{red},0}$ 46 dof
1	1.34 ^{+0.02} _{-0.01}	1.02 ^{+0.03} _{-0.03}	0.3 ^{+0.1} _{-0.3}	1.02 ^{+0.50} _{-0.34}	10.2 ^{+0.3} _{-0.2}	1.3 ^{+0.4} _{-0.5}	0.4 ^{+0.2} _{-0.1}	---	---	---	---	1.34	2.76
2	1.38 ^{+0.02} _{-0.01}	1.22 ^{+0.03} _{-0.03}	0.3 ^{+0.2} _{-0.2}	1.15 ^{+0.75} _{-0.19}	10.0 ^{+0.3} _{-0.2}	1.6 ^{+0.5} _{-0.6}	0.5 ^{+0.1} _{-0.2}	---	---	---	---	0.98	2.10
3	1.42 ^{+0.01} _{-0.01}	1.57 ^{+0.03} _{-0.03}	0.3 ^{+0.2} _{-0.3}	1.32 ^{+0.69} _{-0.38}	9.6 ^{+0.2} _{-0.1}	1.4 ^{+0.6} _{-0.4}	0.5 ^{+0.2} _{-0.1}	---	---	---	---	0.93	2.41
4	1.38 ^{+0.01} _{-0.01}	1.81 ^{+0.04} _{-0.03}	0.0 ^{+0.0} _{-0.0}	1.10 ^{+0.29} _{-0.20}	9.6 ^{+0.1} _{-0.1}	1.2 ^{+0.2} _{-0.2}	0.5 ^{+0.0} _{-0.1}	---	---	---	---	0.68	4.64
5	1.32 ^{+0.01} _{-0.01}	1.82 ^{+0.03} _{-0.03}	0.0 ^{+0.01} _{-0.00}	1.15 ^{+0.26} _{-0.24}	9.8 ^{+0.1} _{-0.1}	0.8 ^{+0.1} _{-0.1}	0.3 ^{+0.0} _{-0.0}	---	---	---	---	0.96	6.57
6	1.28 ^{+0.01} _{-0.01}	1.83 ^{+0.04} _{-0.03}	0.8 ^{+0.1} _{-0.1}	2.75 ^{+0.52} _{-0.47}	10.0 ^{+0.2} _{-0.0}	0.4 ^{+0.2} _{-0.1}	0.2 ^{+0.0} _{-0.0}	---	---	---	---	1.69	5.46
7	1.28 ^{+0.00} _{-0.01}	1.90 ^{+0.03} _{-0.03}	1.0 ^{+0.1} _{-0.2}	2.96 ^{+0.51} _{-0.46}	10.0 ^{+0.1} _{-0.1}	0.3 ^{+0.2} _{-0.3}	0.2 ^{+0.0} _{-0.1}	---	---	---	---	1.41	4.35
8	1.23 ^{+0.01} _{-0.02}	1.84 ^{+0.03} _{-0.04}	0.0 ^{+0.4} _{-0.0}	0.62 ^{+0.26} _{-0.19}	9.7 ^{+0.1} _{-0.1}	1.0 ^{+0.2} _{-0.1}	0.4 ^{+0.1} _{-0.6}	17.5 ^{+0.6} _{-0.4}	2.5	0.8 ^{+0.2} _{-0.2}	1.24	2.29	5.38
9	1.22 ^{+0.02} _{-0.01}	1.85 ^{+0.04} _{-0.04}	0.0 ^{+0.3} _{-0.0}	0.74 ^{+0.49} _{-0.20}	9.3 ^{+0.2} _{-0.1}	1.3 ^{+0.2} _{-0.2}	0.5 ^{+1.0} _{-0.1}	18.4 ^{+0.4} _{-0.4}	2.5	1.0 ^{+0.3} _{-0.2}	1.05	2.80	5.42
10	1.22 ^{+0.03} _{-0.3}	1.85 ^{+0.07} _{-0.08}	0.4 ^{+0.1} _{-0.1}	2.28 ^{+1.14} _{-0.39}	9.8 ^{+0.4} _{-0.4}	2.1 ^{+0.7} _{-0.6}	0.7 ^{+0.4} _{-0.3}	18.7 ^{+0.3} _{-0.4}	2.5	1.3 ^{+0.5} _{-0.3}	1.33	2.81	3.64
11	1.20 ^{+0.03} _{-0.03}	1.78 ^{+0.08} _{-0.08}	0.4 ^{+0.1} _{-0.0}	4.32 ^{+1.16} _{-1.02}	11.5 ^{+0.3} _{-0.3}	2.2 ^{+0.6} _{-0.5}	0.8 ^{+0.5} _{-0.3}	19.1 ^{+0.4} _{-0.5}	2.5	1.5 ^{+0.4} _{-0.5}	1.17	2.17	2.62
12	1.29 ^{+0.01} _{-0.01}	1.94 ^{+0.03} _{-0.03}	0.4 ^{+0.1} _{-0.0}	4.40 ^{+0.68} _{-0.71}	11.8 ^{+0.3} _{-0.3}	1.2 ^{+0.4} _{-0.3}	0.2 ^{+0.1} _{-0.0}	---	---	---	---	1.43	2.58
13	1.28 ^{+0.01} _{-0.01}	1.68 ^{+0.03} _{-0.03}	0.4 ^{+0.1} _{-0.1}	2.44 ^{+0.85} _{-0.69}	11.5 ^{+0.3} _{-0.4}	1.7 ^{+0.7} _{-0.4}	0.4 ^{+0.2} _{-0.1}	---	---	---	---	0.89	2.25
14	1.26 ^{+0.01} _{-0.01}	1.35 ^{+0.03} _{-0.03}	0.3 ^{+0.1} _{-0.3}	1.13 ^{+0.71} _{-0.34}	10.9 ^{+0.3} _{-0.3}	1.8 ^{+0.4} _{-0.4}	0.6 ^{+0.2} _{-0.1}	---	---	---	---	1.03	3.66
15	1.31 ^{+0.01} _{-0.01}	1.15 ^{+0.02} _{-0.03}	0.3 ^{+0.2} _{-0.2}	1.18 ^{+0.45} _{-0.27}	10.5 ^{+0.2} _{-0.2}	1.2 ^{+0.3} _{-0.3}	0.4 ^{+0.1} _{-0.1}	---	---	---	---	1.02	3.49
16	1.34 ^{+0.02} _{-0.01}	1.00 ^{+0.03} _{-0.02}	0.3 ^{+0.2} _{-0.1}	1.31 ^{+0.46} _{-0.34}	10.2 ^{+0.2} _{-0.2}	0.8 ^{+0.4} _{-0.3}	0.3 ^{+0.1} _{-0.1}	---	---	---	---	0.99	2.38

NOTE. — α and β are respectively the normalization constants of the cut-off power law and Gaussian iron emission line; $E_{\text{cyc},1}$, $\sigma_{\text{cyc},1}$, and $\tau_{\text{cyc},1}$ the energy, width, and Gaussian optical depth of the first CRSF; $E_{\text{cyc},2}$, $\sigma_{\text{cyc},2}$, and $\tau_{\text{cyc},2}$ the same parameters for the second CRSF; $\chi_{\text{red},0}$, $\chi_{\text{red},1}$, and $\chi_{\text{red},2}$ the reduced χ^2 values for fits with no CRSF, one (the fundamental) CRSF, and both CRSFs. ^aUnits are 10^{-1} photons keV⁻¹ cm⁻² at 1 keV. ^bUnits are 10^{-3} total photons cm⁻² s⁻¹ in the line.